Molecular Crystals and Liquid Crystals Incorporating Nonlinear Optics

Publication details, including instructions for authors and subscription information:
http://www.tandfonline.com/loi/gmcl17

Diamagnetic to Paramagnetic Transition in Trisdimethylaminocyclopropenium Tetracyanoquinodimethanide (TDAC-TCNQ)

T. P. Radhakrishnan [b] , D. Van Engen [a] & Z. G. Soos [a]

[a] Department of Chemistry, Princeton University, Princeton, NJ, 08544

[b] Department of Chemistry, University of Texas at El Paso, El Paso, Texas, 79968

Version of record first published: 13 Dec 2006.

To cite this article: T. P. Radhakrishnan , D. Van Engen & Z. G. Soos (1987): Diamagnetic to Paramagnetic Transition in Trisdimethylaminocyclopropenium Tetracyanoquinodimethanide (TDAC-TCNQ), Molecular Crystals and Liquid Crystals Incorporating Nonlinear Optics, 150:1, 473-492

To link to this article: http://dx.doi.org/10.1080/00268948708074815

Mol. Cryst. Liq. Cryst., 1987, Vol. 150b, pp. 473–492
Photocopying permitted by license only

Printed in the United States of America

Diamagnetic to Paramagnetic Transition in Trisdimethylaminocyclopropenium Tetracyanoquinodimethanide (TDAC-TCNQ)

T. P. RADHAKRISHNAN,† D. VAN ENGEN and Z. G. SOOS

Department of Chemistry, Princeton University, Princeton, NJ 08544

(*Received February 18, 1987; in final form June 3, 1987*)

Two crystalline forms of TDAC-TCNQ obtained under different crystallization conditions are both stable at room temperature. The diamagnetic yellow form belongs to the triclinic space group $P\bar{1}$, with unit cell parameters a = 7.030(2), b = 8.791(2), c = 17.306(6) Å, α = 94.23(3)°, β = 101.24(3)°, γ = 90.95(2)°, V = 1045.7(6) Å^3 and Z = 1 (R_w = 0.073); it also has a long σ-bond between $TCNQ^-$ in adjacent stacks, but shows no thermally activated triplets. The paramagnetic black form belongs to the monoclinic space group $P2_{1/c}$, with unit cell parameters a = 17.536(4), b = 7.272(2), c = 17.776(4) Å, β = 113.36(2)°, V = 2081.2(9) Å^3 and Z = 4 (R_w = 0.058); it corresponds to a mixed stack of closed shell $TDAC^+$ ions and $TCNQ^-$ ion-radicals. Heating the yellow crystal above 79 ± 3°C converts it to the black form. Subsequent cooling below −50 ± 10°C regains the yellow form with paramagnetic $TCNQ^-$ defects. The hysteresis is interpreted in terms of a high activation barrier for the large (>2 Å) molecular motion of each $TCNQ^-$, in contrast to the unactivated, small amplitude (<0.2 Å) motions associated with spin-Peierls transitions.

Keywords: TCNQ complexes, magneto-structural transition

1. INTRODUCTION

Molecular solids of π-electron donors (D), π-acceptors (A), or metallomacrocyclic π-ligands (ML) often crystallize in face-to-face

†Present address: Department of Chemistry, University of Texas at El Paso, El Paso, Texas 79968.

stacks leading to one-dimensional magnetic, electric, or optical excitations. Isostructural series[1,4] delineate systematic variations or common features. Minor chemical changes, on the other hand, sometimes produce enormous structural changes[5] as illustrated by 1:1 charge-transfer (CT) complexes of substituted phenazine (RP or R_2P) donors and tetracyanoquinodimethane (TCNQ). Van der Waals interactions are maximized in space-filling structures, which can be satisfied almost equally well by several arrangements of conjugated molecules or ions. Additional small intermolecular forces (dispersion, H-bonding, charge-transfer, etc.) compete on almost equal footing.[6] The large electrostatic (Madelung) energy of π-ionic solids barely balances the I-A energy for ionizing (I) good donors and transferring the electron (A) to a good acceptor. The 1:1 TCNQ complex with the D_{3h} ion, trisdimethylaminocyclopropenium (TDAC), was prepared as part of our search[7] for organic ferromagnetism based on superexchange through symmetric closed-shell spacers.

We present here the structure and magnetism of the two phases of the TDAC-TCNQ complex: a diamagnetic yellow form containing σ-bonded $TCNQ^-$ dimers and a paramagnetic black form with isolated $TCNQ^-$ radicals. Both have mixed . . . $D^+A^-D^+A^-$ . . . stacks of $TDAC^+$ and $TCNQ^-$. As in the ethylphenazine (EP) complex,[8] a long σ-bond forms between $TCNQ^-$ in adjacent stacks in the yellow form. Heating the yellow material above 79 ± 3°C or cooling the black material below −50 ± 10°C interconverts them as described below.

Transitions from low to high paramagnetism are expected as dimerized arrays become regular. Bray *et al.*[9] review several spin-Peierls systems, where the driving force for dimerization is the gain in exchange energy. The transition temperature is low, $T_c < 20$ K; triplet spin excitons (TSE) are found below T_c and the exchange J is an order of magnitude larger than kT_c. Similar transitions have been observed in TCNQ salts[10] with K^+, Na^+ and NH_4^+ and in TMPD-ClO_4; in the latter the transition also involves the onset of ClO_4 rotation. Torrance[11] has suggested that these and other systems, with still higher T_c, have generalized spin-Peierls transitions even though linear changes in J are no longer sufficient by themselves. The K-Chloranil complex[12] represents still another variation, with transitions at 260 K on heating and 210 K on cooling and no TSE signals even at low temperature where the susceptibility is activated. The hysteresis is still larger in TDAC-TCNQ. The dimerization amplitude of some 2 Å is more than an order of magnitude greater than in K-TCNQ or in TMPD-ClO_4. The exchanges are consequently far

from linear, with $2J < 30$ cm^{-1} in the black form and >4000 cm^{-1} in the yellow form.

Crystal structures of tris (3,5-di-tert-butylphenyl) methyl radical and its dimer, namely, hexakis (3,5-di-tert-butylphenyl) ethane have been determined recently.[13] The crystals were grown from different solvents that were included in the respective crystal lattices. The colorless dimer on heating turns into the red monomer by breakage of the long (1.67 Å) σ-bond, and the associated change in magnetism is seen in the sudden rise of the EPR signal intensity,[14] in a manner analogous to TDAC-TCNQ. The essential difference is the inclusion of different solvent molecules in the two forms.

2. EXPERIMENTAL

A. Preparation

TDAC-TCNQ was prepared by the metathesis reaction of TDAC-$BF_4 \cdot 1/2\ H_2O$ and LiTCNQ.

TDAC-$BF_4 \cdot 1/2\ H_2O$ was prepared according to Harris and Gray.[15] LiTCNQ was prepared by the reduction[16] of TCNQ with LiI. Equivalent amounts of TDAC-$BF_4 \cdot 1/2\ H_2O$ and LiTCNQ were dissolved separately in minimum amount of deaerated distilled water and the filtered solutions were mixed and stirred. The thick precipitate of TDAC-TCNQ formed was immediately filtered out and washed several times with distilled water. Vacuum drying for 4–5 hours gave a light green solid. This powder was recrystallized in two different ways to yield two crystalline forms.

Solution of 15 mg TDAC-TCNQ in 4 mL acetone was mixed with equal volume of distilled deaerated water. The solution was taken in a stoppered flask and a slow nitrogen flush was introduced through the stopper. In a few hours when most of the acetone has evaporated, long yellow needles were suspended in water. The crystals were filtered out, washed with water and vacuum dried at room temperature for several hours. When these yellow crystals are heated to ~80°C, they were found to change color to black, with concomitant changes in magnetic properties. The black form of TDAC-TCNQ was crystallized from solution as follows.

15 mg of TDAC-TCNQ was dissolved in 10 mL acetonitrile and the solution mixed with 5 mL of xylene. The mixed solution was heated in a silicon fluid bath at ~100°C. In a few hours, when all the acetonitrile had evaporated off, black needles were obtained in xy-

lene. The crystals were filtered out, washed with xylene and vacuum dried for several hours (sample for chemical analysis was dried under vacuum at ~100°C).

The theoretically calculated chemical composition for a 1:1 complex $[C_9H_{18}N_3]^+[C_{12}H_4N_4]^-$ is C–67.72%, H–5.95% and N–26.33% and applies to both the yellow and black forms. The composition found for two differently crystallized black samples were C–67.41, 66.94%, H–5.65, 5.44% and N–26.18, 25.97%. Yellow samples could not be dried at high temperatures due to interconversion to the black form. The analytical data is C–66.74%, H–5.21% and N–25.72%.

B. Crystal structure

A needle-shaped single crystal was mounted on a glass fiber and centered on a Nicolet R3m diffractometer. Cell constants and their esd's were determined by a least-squares fit of diffractometer-measured reflections with $40° \leq 2\theta \leq 45°$. The crystal parameters are collected in Table I.

TABLE I

Comparison of yellow and black forms of TDAC-TCNQ

a. Crystal parameters	Yellow form	Black form
Crystal size (mm)	0.06 × 0.08 × 0.45	0.02 × 0.05 × 0.37
a(Å)	7.030(2)	17.536(4)
b(Å)	8.791(2)	7.272(2)
c(Å)	17.306(6)	17.776(4)
α(°)	94.23(3)	90.00(0)
β(°)	101.24(3)	113.36(2)
γ(°)	90.95(2)	90.00(0)
V(Å^3)	1045.7(6)	2081.2(9)
Z	1	4
Space Group	$P\bar{1}$	$P2_{1/c}$
ρ(calc) (g cm^{-3})	1.18	1.19
F(000)	394	788
b. Data measurements		
2θ range (°)	3–105	3–100
Scan width	0.75	1.00
Unique reflections	2409	2141
Observed reflections	1814	1173
Parameters	253	253
R	0.064	0.080
R_w	0.073	0.058
GOF	1.36	1.64

All intensity measurements were made at room temperature using graphite-monochromated CuKα radiation (λ = 1.54178 Å) and an ω-scan technique with a variable scan rate of 3.91 – 29.30°/min. Background counts were taken for half the scan time at each extreme of the scan range. All data (2513 having $l \geq 0$ for the yellow form and 2461 having $k, l \geq 0$ for the black form) were measured in this manner. Crystal decomposition was monitored throughout the data collection by remeasuring two standard reflections after every 50 data measurements; no significant variation in intensity was observed. The intensities were reduced by applying Lorentz and polarization corrections. Systematically absent reflections were eliminated and equivalent reflections were averaged to give unique data; those with $|F_0| > 3\sigma(F_0)$ were considered observed (Table I).

The structure was solved by direct methods using the SHELXTL software. Following refinement of the nonhydrogen atoms with anisotropic temperature factors, a difference Fourier map displayed peaks at plausible hydrogen positions. The hydrogen atoms were subsequently included in refinement in ideal positions (C—H 0.96 Å, CCH 109° or 120°). In the final cycles of blocked-cascade least-squares refinement, the nonhydrogen atoms were refined with anisotropic temperature factors and the hydrogens were varied using a riding model. When the refinement converged (shift/error ≤ 0.10), no peaks of any consequence were observed in the final difference map (max e/Å^3 = 0.22 and 0.24 for the yellow and black forms, respectively). The quantity minimized by the least-squares program was $\Sigma w(|F_0| - |F_c|)^2$ where w is the weight of the given observation ($w = [\sigma^2(|F_0|) + g|F_0|^2]^{-1}$) with $g = 0.0022$ and 0.00001 for the yellow and black forms, respectively. The analytical forms for the scattering factors of the neutral atoms were used.[17]

C. Electron paramagnetic resonance

EPR spectra were run on a standard Varian E12 spectrometer operating at the X-band (~9 GHz) with 100 kHz modulation of the magnetic field. Spectra were collected from −150°C to 120°C; temperature variation was done with a Varian E-257 variable temperature accessory.

3. RESULTS

The yellow form of TDAC-TCNQ is properly written as $2(TDAC^+)(TCNQ)_2^{2-}$, since the $TCNQ^-$ radical ions in Figure 1(a)

form a long (1.62 Å) σ-bond at C(16).† The resulting pyramidalization is clearly seen in Figure 2, which shows the crystal packing along the *Y*-axis. The midpoint of the long σ-bond is a center of inversion. The independent unit then consists of one $TDAC^+$ ion and half of the $TCNQ^-$ dimer. The atomic coordinates in Table II correspond to

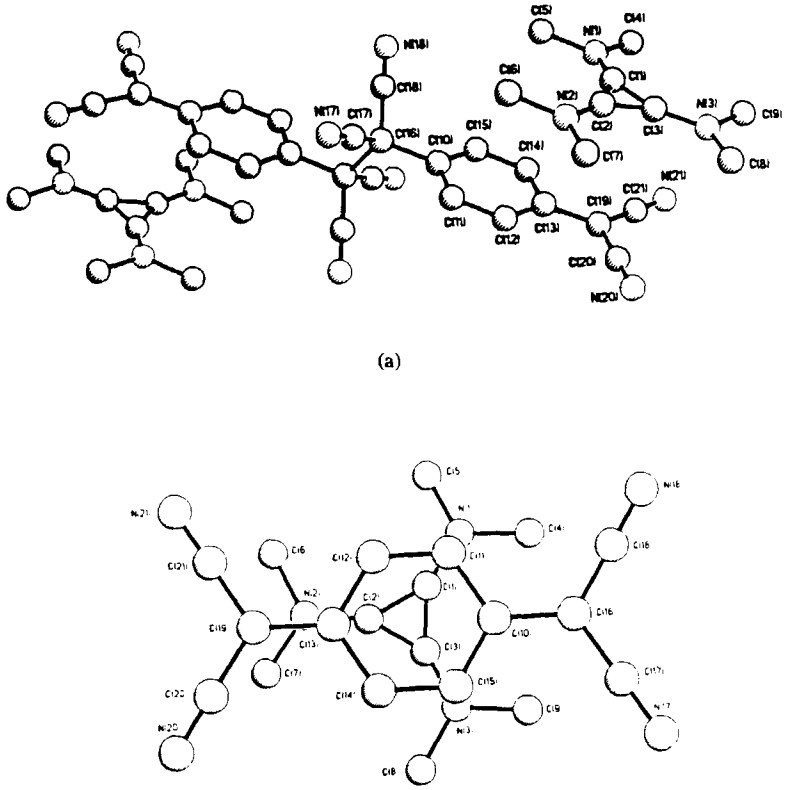

(a)

(b)

FIGURE 1 (a) Pluto-type drawing of $2(TDAC^+)(TCNQ)^{2-}$ in the yellow form of TDAC-TCNQ with $TDAC^+$ and one half of the TCNQ dimer labelled; (b) Pluto-type drawing of $TDAC^+$ and $TCNQ^-$ in the black form of TDAC-TCNQ; atom labellings are shown.

†Ortep drawings with anisotropic thermal ellipsoids for Figure 1(a) and (b) are available on request.

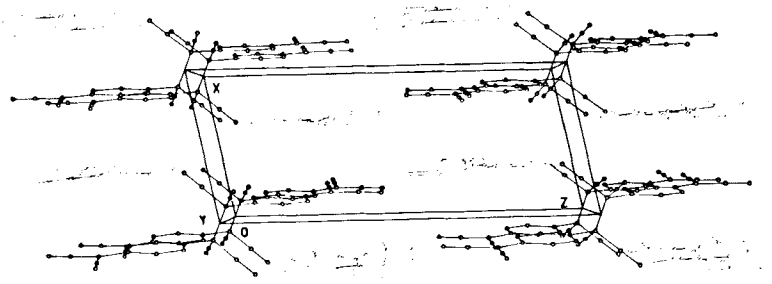

FIGURE 2 Unit cell packing diagram of the yellow form of TDAC-TCNQ viewed down the *Y*-axis.

TABLE II

Atomic coordinates ($\times 10^4$) and isotropic thermal parameters ($Å^2 \times 10^3$) in the yellow form of TDAC-TCNQ (labelling of atoms as in Figure 1(a))

	x	*y*	*z*	*U*
C(1)	6678(5)	−3177(4)	2628(2)	63(1)*
C(2)	6544(6)	−1866(4)	3090(2)	74(2)*
C(3)	6800(6)	−3222(4)	3426(2)	73(2)*
N(1)	6653(5)	−3883(4)	1927(2)	74(1)*
C(4)	6881(7)	−5520(5)	1836(3)	102(2)*
C(5)	6517(6)	−3043(5)	1228(2)	85(2)*
N(2)	6261(7)	−390(4)	3166(2)	109(2)*
C(6)	6226(8)	545(5)	2505(3)	106(2)*
C(7)	6250(16)	361(6)	3938(4)	213(5)*
N(3)	7030(6)	−4004(4)	4062(2)	93(2)*
C(8)	7122(8)	−3225(7)	4834(3)	123(3)*
C(9)	7400(9)	−5603(5)	3991(3)	123(3)*
C(10)	1260(5)	−932(4)	991(2)	51(1)*
C(11)	1138(5)	−240(4)	1723(2)	64(1)*
C(12)	1278(6)	−1097(4)	2370(2)	69(2)*
C(13)	1549(5)	−2671(4)	2317(2)	60(1)*
C(14)	1662(5)	−3346(4)	1568(2)	59(1)*
C(15)	1537(5)	−2492(4)	923(2)	54(1)*
C(16)	1093(5)	5(4)	263(2)	51(1)*
C(17)	1699(5)	1603(4)	499(2)	58(1)*
N(17)	2120(5)	2856(4)	677(2)	80(1)*
C(18)	2354(5)	−619(4)	−270(2)	55(1)*
N(18)	3307(5)	−1128(4)	−672(2)	77(1)*
C(19)	1751(6)	−3565(4)	2992(2)	70(2)*
C(20)	1738(6)	−2832(5)	3744(2)	86(2)*
N(20)	1715(7)	−2220(5)	4352(2)	121(2)*
C(21)	2039(7)	−5138(6)	2943(2)	82(2)*
N(21)	2268(8)	−6419(5)	2896(3)	125(2)*

*Equivalent isotropic *U* defined as one third of the trace of the orthogonalised U_{ij} tensor.

the labelling in Figure 1(a). Bond lengths and angles are collected in Table III.

The $(TCNQ)_2^{2-}$ dimers in Figure 2 stack along [100], which is within 4° of the perpendicular to the molecular planes. There is one dimer

TABLE III

Bond lengths (Å) and angles (deg) in the yellow form of TDAC-TCNQ (labelling of atoms as in Figure 1(a))

$TDAC^+$		$TCNQ^-$	
C(1)—C(2)	1.369(5)	C(10)—C(15)	1.388(4)
C(1)—N(1)	1.318(5)	C(11)—C(12)	1.384(5)
C(2)—N(2)	1.318(5)	C(13)—C(14)	1.401(5)
N(1)—C(4)	1.451(5)	C(14)—C(15)	1.381(5)
N(2)—C(6)	1.453(6)	C(16)—C(18)	1.482(5)
N(3)—C(8)	1.445(6)	C(17)—N(17)	1.140(4)
C(1)—C(3)	1.370(5)	C(19)—C(20)	1.410(5)
C(2)—C(3)	1.363(5)	C(20)—N(20)	1.150(5)
C(3)—N(3)	1.326(5)	C(10)—C(11)	1.383(4)
N(1)—C(5)	1.452(5)	C(10)—C(16)	1.542(4)
N(2)—C(7)	1.447(7)	C(12)—C(13)	1.399(5)
N(3)—C(9)	1.434(6)	C(13)—C(19)	1.442(5)
		C(16)—C(17)	1.467(4)
		C(16)—C(16′)	1.626(6)
		C(18)—N(18)	1.132(5)
		C(19)—C(21)	1.400(6)
		C(21)—N(21)	1.139(7)
C(2)—C(1)—C(3)	59.7(3)		
C(3)—C(1)—N(1)	150.1(4)		
C(1)—C(2)—N(2)	150.6(4)		
C(1)—C(3)—C(2)	60.1(3)		
C(2)—C(3)—N(3)	149.8(4)	C(11)—C(10)—C(15)	118.6(3)
C(1)—N(1)—C(5)	121.3(3)	C(15)—C(10)—C(16)	120.5(3)
C(2)—N(2)—C(6)	120.9(4)	C(11)—C(12)—C(13)	122.2(3)
C(6)—N(2)—C(7)	118.6(4)	C(12)—C(13)—C(19)	122.6(3)
C(3)—N(3)—C(9)	119.5(4)	C(13)—C(14)—C(15)	121.5(3)
C(2)—C(1)—N(1)	150.2(4)	C(10)—C(16)—C(17)	111.0(2)
C(1)—C(2)—C(3)	60.2(3)	C(17)—C(16)—C(18)	107.9(3)
C(3)—C(2)—N(2)	149.1(4)	C(17)—C(16)—C(16′)	107.3(3)
C(1)—C(3)—N(3)	150.1(4)	C(16)—C(17)—N(17)	178.2(4)
C(1)—N(1)—C(4)	121.0(3)	C(13)—C(19)—C(20)	119.4(4)
C(4)—N(1)—C(5)	117.6(3)	C(20)—C(19)—C(21)	117.8(4)
C(2)—N(2)—C(7)	120.0(4)	C(19)—C(21)—N(21)	179.4(4)
C(3)—N(3)—C(8)	120.3(4)	C(11)—C(10)—C(16)	120.9(3)
C(8)—N(3)—C(9)	119.9(4)	C(10)—C(11)—C(12)	120.3(3)
		C(12)—C(13)—C(14)	116.4(3)
		C(14)—C(13)—C(19)	121.0(3)
		C(10)—C(15)—C(14)	121.0(3)
		C(10)—C(16)—C(18)	110.3(3)
		C(10)—C(16)—C(16′)	113.4(3)
		C(18)—C(16)—C(16′)	106.6(3)
		C(16)—C(18)—N(18)	178.4(4)
		C(13)—C(19)—C(21)	122.8(3)
		C(19)—C(20)—N(20)	179.1(5)

per unit cell. Each dimer in Figure 2 participates in two mixed regular stacks with $TDAC^+$ ions. The mean molecular planes of $TDAC^+$ and $TCNQ^-$ are within 3.6° of being parallel and are separated by 3.43 Å. The centroid–centroid distance between the rings is 4.15 Å. The interplanar separation is slightly below the typical Van der Waal's separation of 3.5–3.6 Å for stacked π-clouds.

Dimerization of $TCNQ^-$ ion radicals removes the spins. Yellow crystals show a weak, asymmetric EPR signal around $g = 2.0023$ that we attribute to defects. Three previous examples of σ-bonded $TCNQ^-$ dimers[8,18,19] showed fine structure splittings typical of triplet spin excitons (TSE) corresponding to broken bonds. We searched carefully for TSE splittings by heating the crystal to increase the equilibrium density of TSE's. No TSE signals were found. At $T = 79 \pm 3$°C, however, the $g = 2$ EPR signal increased in intensity by a hundred-fold and the crystal turned to deep black. These changes are attributed below to the cooperative breakage of all σ-bonds.

Black $(TDAC^+)(TCNQ^-)$ crystals contain mixed stacks of diamagnetic cations and paramagnetic anions whose overlap is shown in Figure 1(b)†. Atomic coordinates in Table IV refer to the atoms labelled in Figure 1(b) and the bond lengths and angles are given in Table V. The unit cell packing viewed along the Z-axis in Figure 3 shows four chemically equivalent, nearly regular mixed stacks in which the mean $TDAC^+$ and $TCNQ^-$ planes are parallel within experimental error (0.14°). The smallest centroid–centroid distance between a cation and anion is 3.53 Å. The separations between the mean molecular planes of the cation and adjacent anions in the stack are 3.458 Å and 3.477 Å respectively.

The black crystals are strongly paramagnetic, with 1.0 ± 0.1 spins per $TCNQ^-$ obtained by comparing the EPR signal intensity to that of a standard DPPH sample. The intensity of the single, exchange-narrowed Lorentzian line of 0.5–0.6 G width and $g \sim 2$, follows a Curie law between −50° and 120°C. Any exchange is small, with $J < 50$ K, and consistent with essentially one spin per $TCNQ^-$. The g-tensors of both black and yellow crystals have typical $TCNQ^-$ values. Accurate susceptibility measurements are hampered for $T >$ 120° by sample decomposition and for $T < -50$°C by a phase change (Figure 4) involving the loss of 90–95% of the EPR intensity. Although there is no marked color change, we interpret the loss as reversion to σ-bonded $TCNQ^-$ dimers in the yellow form.

As shown in Figure 4, the weak paramagnetism of yellow crystals changes around $T = 79 \pm 3$°C to the strong paramagnetism of the black form. Subsequent cooling leads to identical behavior, within experimental accuracy, to that of crystals prepared in the black form.

TABLE IV

Atomic coordinates ($\times 10^4$) and isotropic thermal parameters ($Å^2 \times 10^3$) in the black form of TDAC-TCNQ (labelling of atoms as in Figure 1(b))

	x	y	z	U
C(1)	2772(4)	6439(10)	9790(4)	50(3)*
C(2)	1961(4)	5869(9)	9323(4)	54(4)*
C(3)	2180(3)	6347(9)	10118(3)	54(3)*
N(1)	3532(3)	6778(8)	9873(3)	70(3)*
N(2)	1422(4)	5308(9)	8599(3)	76(3)*
N(3)	1973(3)	6520(8)	10752(3)	71(3)*
C(4)	4170(4)	7304(11)	10663(4)	101(5)*
C(5)	3750(4)	6695(12)	9169(4)	120(5)*
C(6)	1671(4)	5062(11)	7912(4)	105(5)*
C(7)	559(4)	5038(11)	8465(4)	105(5)*
C(8)	1124(4)	6166(11)	10678(4)	101(5)*
C(9)	2580(4)	7066(10)	11550(3)	91(4)*
C(10)	3280(3)	2669(9)	6319(3)	50(3)*
C(11)	3427(4)	2925(9)	5589(3)	55(3)*
C(12)	2816(3)	3505(9)	4889(3)	62(3)*
C(13)	2002(4)	3887(9)	4827(4)	52(4)*
C(14)	1851(4)	3584(9)	5553(4)	60(4)*
C(15)	2467(3)	2986(9)	6253(3)	60(3)*
C(16)	3930(3)	2126(10)	7060(3)	60(3)*
C(17)	3795(4)	1947(10)	7798(4)	69(3)*
N(17)	3688(3)	1746(10)	8389(3)	101(3)*
C(18)	4749(4)	1877(13)	7129(4)	70(4)*
N(18)	5411(3)	1645(9)	7179(3)	106(3)*
C(19)	1377(4)	4549(10)	4099(4)	59(4)*
C(20)	568(4)	5018(10)	4050(4)	68(4)*
N(20)	−74(3)	5396(9)	4012(3)	94(3)*
C(21)	1517(4)	4837(10)	3378(4)	69(4)*
N(21)	1611(3)	5039(9)	2784(3)	107(4)*

*Equivalent isotropic U defined as one third of the trace of the orthogonalised U_{ij} tensor

The sharpness in the intensity changes in Figure 4 depends on careful heating and equilibration of crystals. Powder samples showed only the features of the onset of paramagnetism at $T \sim 80°C$ and its lowering at $T \sim -50°C$; their residual paramagnetism on cooling was consistently higher.

Crystallographic efforts to demonstrate yellow–black interconversion were unsuccessful. Although gentle heating of yellow crystals produced apparently intact black samples, rotation photographs immediately showed them not to be single crystals. Careful prolonged cooling of black crystals produced the same outcome. The molecular motions that interconvert the two TDAC-TCNQ forms are evidently too large to preserve the integrity of single crystals. We pursue below the nature of these molecular motions.

TABLE V

Bond lengths (Å) and angles (deg) in the black form of TDAC-TCNQ (labelling of atoms as in Figure 1(b))

$TDAC^+$		$TCNQ^-$	
C(1)—C(2)	1.395(9)	C(10)—C(15)	1.403(8)
C(1)—N(1)	1.305(10)	C(11)—C(12)	1.348(7)
C(2)—N(2)	1.324(7)	C(13)—C(14)	1.433(11)
N(1)—C(4)	1.458(7)	C(14)—C(15)	1.355(7)
N(2)—C(6)	1.462(10)	C(16)—C(18)	1.404(10)
N(3)—C(8)	1.465(9)	C(18)—N(18)	1.142(10)
C(1)—C(3)	1.378(11)	C(19)—C(21)	1.412(11)
C(2)—C(3)	1.354(9)	C(21)—N(21)	1.141(10)
C(3)—N(3)	1.319(9)	C(10)—C(11)	1.432(9)
N(1)—C(5)	1.449(10)	C(10)—C(16)	1.414(7)
N(2)—C(7)	1.448(9)	C(12)—C(13)	1.414(10)
N(3)—C(9)	1.451(7)	C(13)—C(19)	1.408(8)
		C(16)—C(17)	1.427(10)
		C(17)—N(17)	1.148(9)
		C(19)—C(20)	1.428(11)
		C(20)—N(20)	1.134(10)
C(2)—C(1)—C(3)	58.5(5)		
C(3)—C(1)—N(1)	150.2(6)		
C(1)—C(2)—N(2)	146.8(8)		
C(1)—C(3)—C(2)	61.4(5)		
C(2)—C(3)—N(3)	148.7(6)	C(11)—C(10)—C(15)	116.4(5)
C(1)—N(1)—C(5)	120.2(5)	C(15)—C(10)—C(16)	122.7(6)
C(2)—N(2)—C(6)	121.0(6)	C(11)—C(12)—C(13)	122.8(6)
C(6)—N(2)—C(7)	119.0(5)	C(12)—C(13)—C(19)	122.2(7)
C(3)—N(3)—C(9)	121.2(5)	C(13)—C(14)—C(15)	120.8(6)
C(2)—C(1)—N(1)	151.3(7)	C(10)—C(16)—C(17)	121.1(6)
C(1)—C(2)—C(3)	60.1(5)	C(17)—C(16)—C(18)	116.3(5)
C(3)—C(2)—N(2)	153.1(8)	C(16)—C(18)—N(18)	178.8(8)
C(1)—C(3)—N(3)	149.8(5)	C(13)—C(19)—C(21)	122.1(7)
C(1)—N(1)—C(4)	121.2(6)	C(19)—C(20)—N(20)	179.8(9)
C(4)—N(1)—C(5)	118.5(6)	C(11)—C(10)—C(16)	120.9(6)
C(2)—N(2)—C(7)	119.9(7)	C(10)—C(11)—C(12)	120.9(6)
C(3)—N(3)—C(8)	121.4(5)	C(12)—C(13)—C(14)	116.1(5)
C(8)—N(3)—C(9)	117.5(6)	C(14)—C(13)—C(19)	121.7(7)
		C(10)—C(15)—C(14)	122.8(6)
		C(10)—C(16)—C(18)	122.4(6)
		C(16)—C(17)—N(17)	177.9(8)
		C(13)—C(19)—C(20)	122.0(7)
		C(20)—C(19)—C(21)	115.8(5)
		C(19)—C(21)—N(21)	178.0(6)

4. DISCUSSION

Triplet spin excitons (TSE) were observed at or above room temperature in all three previously studied crystals with σ-bonded $TCNQ^-$ dimers. The singlet–triplet splitting ΔE corresponds to the effective bond strength. Since TSE concentration of $\exp(-\Delta E/kT) < 0.1\%$ is readily detectable by EPR, one explanation for the absence of a TSE

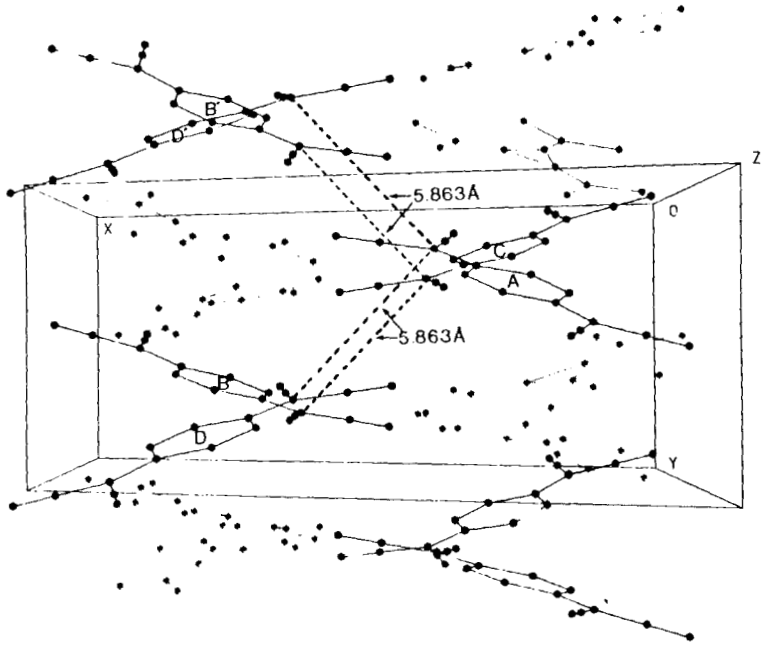

FIGURE 3 Unit cell packing diagram of the black form of TDAC-TCNQ viewed down the Z-axis.

signal is a large ΔE. The σ-bond length of 1.626(6) Å in form of $TDAC^{+}TCNQ^{-}$ is marginally shorter than the 1.631 Å bond in the ethylphenazine complex[8] ($\Delta E = 0.27$ eV), the 1.65 Å bond in the $Pt(2,2'\text{-dipy})_2$ complex[18] ($\Delta E = 0.25$ eV), or the 1.630 Å bond in the $Cu(DMP)_2$ complex[19] ($\Delta E = 0.55$ eV). The TSE signals are interpreted in terms of a few isolated, and possibly mobile, broken σ-bonds. The gray-green $Pt(2,2'\text{-dipy})_2$ complex[18,20] also undergoes a transition at 87°C to a strongly paramagnetic grass-green form that has no TSE signals, but the high temperature structure was not reported.

The interconversion of the magnetism of the yellow and black forms of TDAC-TCNQ, as shown in Figure 4 above, provides the basis for interpreting the 79 ± 3°C transition as the cooperative breaking of all σ-bonds. The bonds are reformed on cooling to −50°C, except for some 5–10% of $TCNQ^{-}$ ions whose neighbors found other partners (see below). Fewer such misfits are seen at $g = 2$ in the directly prepared yellow crystals. The absence of TSE splittings is not due to a larger ΔE than found in the related systems, in our opinion, but is

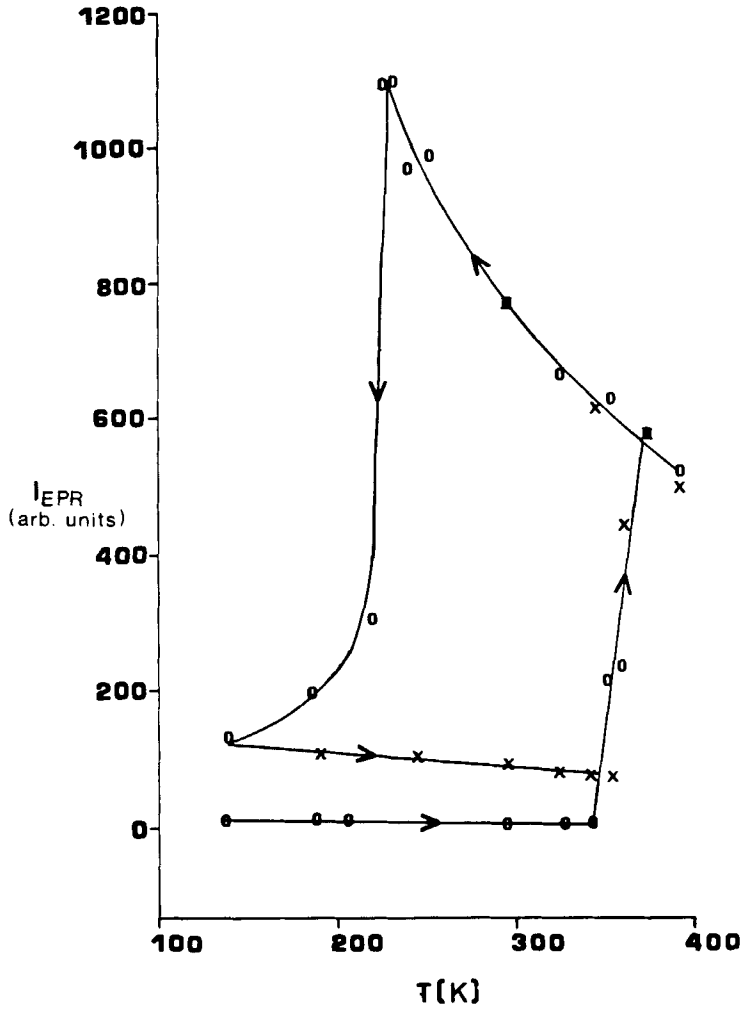

FIGURE 4 Plot of EPR signal intensity against temperature for TDAC-TCNQ. The circles (○) represent the first cycle of heating and cooling and the crosses (×) the second one.

consistent with cooperativity. Breaking a σ-bond may sufficiently weaken neighboring bonds to produce, in effect, nucleation centers for the paramagnetic phase. Such clusters would produce complicated fine structure patterns around $g = 2$ and would be difficult to detect. We can clearly exclude isolated broken σ-bonds.

The weakly interacting $TCNQ^-$ spins in the black form decrease

the molar free energy by RTln2. The yellow form is favored by the σ-bonds. Although the black form has van der Waal's contacts among $TDAC^+$ and $TCNQ^-$, it has a slightly higher density than the σ-bonded (yellow) form (Table I). Crystal packing thus slightly favors the black form. Both structures are stable indefinitely at room temperature.

We consider next the molecular motions for the interconversion of the yellow and black forms. Figure 5(a) and (b) show the projection of the yellow and black structures, respectively, along the stacking axis (*X* for yellow and *Y* for black). On going from black to the yellow form, the unit cell length along the stacking axis (Table I) changes very little; the small decrease is probably due to the molecular planes becoming parallel. The other two unit cell constants in the black form (Figure 5(b)) are about 17.5 Å each (Table I), due to geometric (crystallographic) dimerizations. As shown in Figure 3, the molecular planes are alternately tilted along the *Z*-axis and related by an inversion along the *X*-axis. In the yellow form, on the other hand, there is no geometric dimerization in any direction and all molecular planes are parallel. But the chemical dimerization due to σ-bond formation between $TCNQ^-$ ions, makes the unit cell length along the *Z*-direction of the order of 17.3 Å, whereas *Y*-unit cell constant is approximately half this value (~8.8 Å) (Table I). The unit cell volume of the black form, with the tilted molecular planes, is consequently nearly twice that of the yellow form, which has parallel molecular planes and a σ-bond between the C(16) sites in Figure 1(a). The transformation from black to yellow therefore involves both rotation of the molecular planes and σ-bond formation.

To identify which pairs of $TCNQ^-$ in the black form dimerize to yield the yellow form, we make use of the following criteria: (i) the $TDAC^+$ ions in close contact to the dimerizing $TCNQ^-$ ions must be properly oriented so that in the dimerized version they will be related by a center of inversion (Figure 2); also the separation of the $TDAC^+$ ions must be close to the one found in the yellow structure; (ii) the $TCNQ^-$ ions are then chosen to have the shortest distance between the appropriate methylene carbon atoms (C16 and C19 in Figure 1(b)). The first restriction immediately rules out the dimerizations of A–C or B–D in Figure 5(b), even though the closest methylene carbon separation is 4.669 Å, the shortest available. Using criterion (ii), we prefer A–D and B–C dimerization (methylene carbons 5.863 Å apart) to A–B and C′–D dimerization (methylene carbon separation of 7.448 Å). The separation of the $TDAC^+$ associated with the dimerized $TCNQ^-$ in the yellow form is only ~1

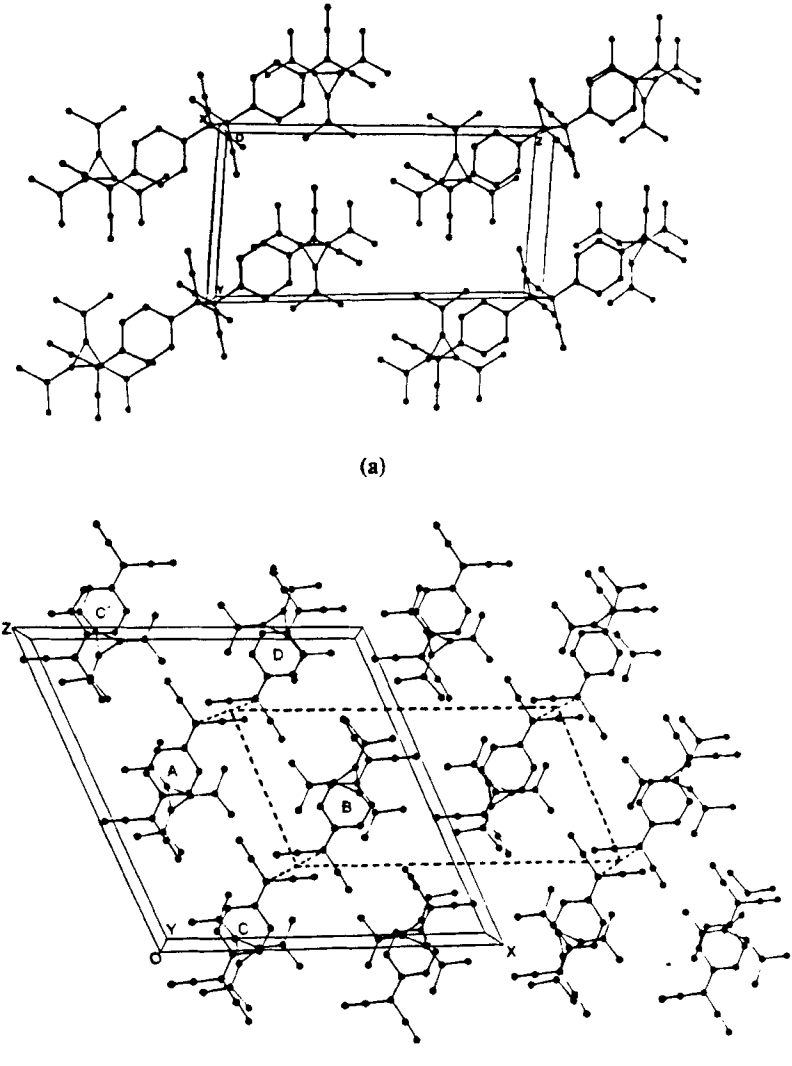

FIGURE 5 (a) Projection of unit cell of the yellow form of TDAC-TCNQ in the *YZ* plane; (b) projection of unit cell of the black form of TDAC-TCNQ in the *XZ* plane. Dashed lines represent schematically the dimerization of $TCNQ^-$ ions and the formation of the cell shown in (a).

Å larger than that of the $TDAC^+$ associated with A–D or B–C pairs, whereas it is ~2 Å larger than the separation of $TDAC^+$ associated with A–B or C′–D pairs.

Now that the $TCNQ^-$ ions A–D and C–B that dimerize have been identified in Figure 5(b), the formation of the yellow form's unit cell in Figure 5(a) can be suggested. Only a suggestion is possible since the unit cells belong to different space groups. The *X*-axis in Figure 5(a) is naturally associated with the *Y*-axis in Figure 5(b). The short edge of the dashed parallelogram in Figure 5(b) becomes the *Y*-axis of the yellow form. The choice of the long edge of the dashed parallelogram for the *Z*-axis of the yellow form almost reproduces the unit cell lengths, but not the angles. Another choice for the *Z*-axis, the shorter diagonal of the parallelogram, is much better for the unit cell angles, but is worse for the length of *Z*.

The magnetic susceptibility of TDAC-TCNQ varies with temperature as shown by the hysteresis curve in Figure 4. The same data is replotted in Figure 6, in terms of the effective number of spins,[21] $\rho = \chi/\chi_{Curie}$, to emphasize the relative susceptibility in the different phases; $\chi_{Curie} = C/T$ is always based on one spin per $TCNQ^-$ ion. The black form represented by line I (Figure 6) from ~ −50°C to 120°C, has $\rho = 1.0 \pm 0.1$, and is a Curie paramagnet within experimental error. As already mentioned, the narrow, Lorentzian EPR signal indicates some exchange, $J < 50$ K, that hardly affects χ at these temperatures. Lines II and III in Figure 6 also follow the Curie law, with $\rho \sim 0.1$ and 0.01, respectively. The latter represents the yellow form with about 1% paramagnetic centers. Line II, on the other hand, represents non-ideal dimerization of $TCNQ^-$, on cooling the black form below −50°C. The unsuitability of this phase for structural analysis is consistent with defects, which on the basis of the paramagnetism are again attributed to misfits in $TCNQ^-$ dimer formation.

One mode of defect formation is suggested by the analysis of the molecular motion for σ-bond formation. As mentioned above, C(16) atoms separated by 5.683 Å probably form σ-bonds, with a concomitant loss of molecular tilts and only slight $TDAC^+$ motion. Only C(16) atoms (Figure 1(b)) form σ-bonds; the C(19) atoms of the $TCNQ^-$ do not, in the proposed mechanism. However, as mentioned in the previous section, the mixed stacking is almost regular along the *Y*-axis, with a small difference in spacings of 0.019(7) Å. As shown in Figure 3, each $TCNQ^-$ has two choices for dimerization that are equivalent (C with B or B′, A with D or D′ etc.). The registry within the uniquely determined columns can thus vary by one. The resulting

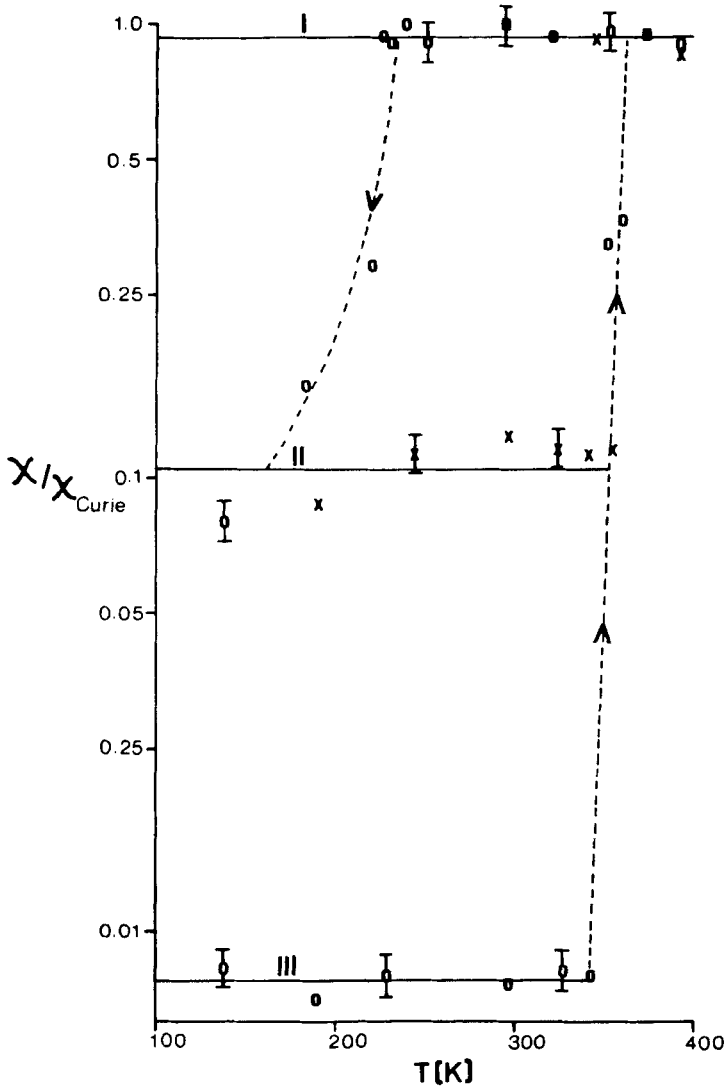

FIGURE 6 Data in Figure 4 replotted as χ/χ_{Curie} versus temperature. Lines I, II, and III are best fits to a Curie law, with effective number of spins, $\rho = 0.933$, 0.105, and 0.008, respectively.

σ-bonds can be tilted in two ways, as shown schematically in Figure 7. For C–B dimerizations, the defect moves to the bottom end of the stack, and for C–B′, it moves to the top end. Equivalent choices exist for the A–D pairs in Figure 3, which are related to the C–B

pairs by an inversion. When the two types of dimerization sequences occur in the same column, the defect (isolated $TCNQ^-$) forms where the registry changes (Figure 7). A sheet of such defects can form in the plane perpendicular to the stack axis, when the registry changes occur at the same point in several neighboring columns. Other extended defect structures can also be conjectured. Available experimental data does not permit a unique choice.

The dimerization at T_c in spin-Peierls systems typically involves molecular motions of <0.2 Å as a regular $\pi-\pi$ stack becomes alternating. Whether or not we adopt linear spin–phonon coupling as the driving force, there is no activation energy and the final dimerization

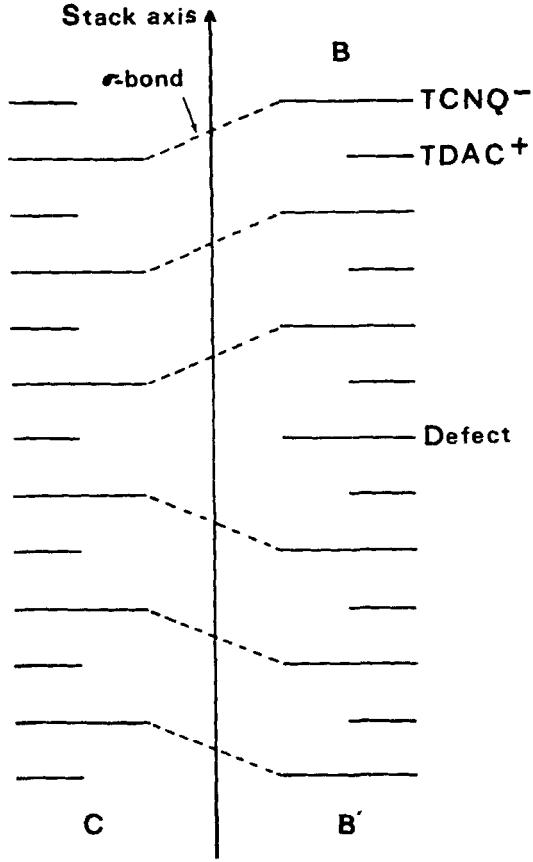

FIGURE 7 Schematic drawing of a $TCNQ^-$ defect formed on cooling black TDAC-TCNQ below -50°C.

depends on lattice strain, exchange, and intermolecular forces. There is no hysteresis. The situation is clearly different for TDAC-TCNQ, where large (>2 Å) molecular motions per $TCNQ^-$ connect the yellow and black form and there is strong hysteresis (Figure 4). The two forms represent free-energy minima separated by an activation barrier whose height is not known. The hysteresis from $-50°C$ to 79°C represents a region of kinetic stability. Either form is stable in this region. Only the black form is stable above 79°C, only the yellow form below $-50°C$. Large molecular motions rationalize high activation energy, highly nonlinear changes in the exchange, and a hysteresis in the generalized spin–Peierls transition. The σ-bond merely contributes to the driving force.

K-Chloranil[12] also shows hysteresis in the susceptibility, although only the high-temperature paramagnetic ($\rho \sim 0.8$) structure is known and the low-temperature phase is activated. There are no TSE signals. Vibrational studies[12b] indicate close similarities between the postulated dimerized form and the H-bonded hydrated structure. The present picture, of misfits rather than TSEs and of large molecular motions, apply qualitatively to this unusual spin–Peierls system. When the driving force for dimerization is not restricted to exchange, a variety of generalized spin–Peierls transitions become possible. In this sense, TDAC-TCNQ illustrates a novel, highly nonlinear case with large-amplitude molecular motions.

Acknowledgments

One of us (TPR) thanks Bart Kahr for stimulating discussions about the long bond in hexaphenylethanes. We gratefully acknowledge financial support for this work under NSF grant DMR-8403819.

References

1. F. Wudl, D. E. Schafer, W. M. Walsh, Jr., L. W. Rupp, F. J. DiSalvo, J. V. Waszczak, M. L. Kaplan and G. A. Thomas, *J. Chem. Phys.*, **66**, 377 (1977).
2. H. J. Pedersen, J. C. Scott and K. Bechgaard, *Phys. Rev.*, **B24**, 5014 (1981).
3. B. M. Hoffmann, J. Martinsen, L. J. Pace and J. A. Ibers, in "Extended Linear Chain Compounds," J. S. Miller (ed.), Vol. 3 (1983), Plenum (New York), p. 459.
4. F. H. Herbstein in "Perspectives in Structural Chemistry," J. D. Dunitz and J. A. Ibers (ed.), Vol. IV (1971), Wiley (New York), p. 166.
5. H. J. Keller and Z. G. Soos, *Topics in Curr. Chem.*, **127**, 169 (1985).
6. (a) R. M. Metzger, in "Crystal Cohesion and Conformational Energies," R. M. Metzger (ed.), Topics in Current Physics, Vol. 26 (1981), Springer (Berlin), p.

80; (b) J. N. Murrell, in "Orbital Theories of Molecules and Solids," N. H. March (ed.), Clarendon (Oxford), 1974, Ch. 7.
7. T. P. Radhakrishnan, Z. G. Soos, H. Endres and L. J. Azevedo, *J. Chem. Phys.*, **85**, 1126 (1986).
8. R. H. Harms, H. J. Keller, D. Nöthe, M. Werner, D. Gundel, H. Sixl, Z. G. Soos and R. M. Metzger, *Mol. Cryst. Liq. Cryst.*, **65**, 179 (1981).
9. J. W. Bray, L. V. Interrante, I. S. Jacobs and J. C. Bonner, in "Extended Linear Chain Compounds," J. S. Miller (ed.), Vol. 3 (1983), Plenum (New York), p. 353.
10. H. Endres, in "Extended Linear Chain Compounds," J. S. Miller (ed.), Vol. 3 (1983), Plenum (New York), p. 263.
11. J. B. Torrance, *Ann. N.Y. Acad. Sci.*, **313**, 210 (1978); *Acc. Chem. Res.*, **12**, 79 (1979).
12. (a) J. J. Andre and G. Weill, *Chem. Phys. Lett.*, **9**, 27 (1971); (b) R. Bozio, A. Girlando and C. Pecile, *Chem. Phys.*, **21**, 257 (1977); (c) A. Kosaki, M. Sorai, H. Suga and S. Seki, *Bull. Chem. Soc. Jap.*, **50**, 810 (1977).
13. B. Kahr, D. Van Engen and K. Mislow, *J. Am. Chem. Soc.*, **108**, 8305 (1986).
14. B. Kahr, private communication.
15. D. C. Harris and H. B. Gray, *Inorg. Chem.*, **13**, 2250 (1974).
16. L. R. Melby, R. J. Harder, W. R. Hertler, W. Mahler, R. E. Benson and W. E. Mochel, *J. Am. Chem. Soc.*, **84**, 3374 (1962).
17. "International Tables of X-ray Crystallography," Kynoch Press, Birmingham, England (1975), Vol. IV, p. 99, 149.
18. V. Dong, H. Endres, H. J. Keller, W. Moroni and D. Nöthe, *Acta Cryst.* **B33**, 2428 (1977).
19. S. K. Hoffmann, P. J. Corvan, P. Singh, C. N. Sethulekshmi, R. M. Metzger and W. E. Hatfield, *J. Am. Chem. Soc.*, **105**, 4608 (1983).
20. H. Endres, H. J. Keller, W. Moroni and D. Nöthe, *Z. Naturforsch*, **31b**, 1322 (1976).
21. Z. G. Soos and D. J. Klein in "Molecular Association," R. Foster (ed.), Vol. 1 (1975), Academic (New York), p. 1.